Equilibrium similarity, effects of initial conditions and local Reynolds number on the axisymmetric wake

Peter B. V. Johansson[a] and William K. George
Department of Thermo and Fluid Dynamics, Chalmers University of Technology, SE-412 96 Gothenburg, Sweden

Michael J. Gourlay
Colorado Research Associates Division/Northwest Research Associates, Inc., 3380 Mitchell Lane, Boulder, Colorado 80302

(Received 30 October 2002; accepted 18 November 2002; published 22 January 2003)

Equilibrium similarity considerations are applied to the axisymmetric turbulent wake, without the arbitrary assumptions of earlier theoretical studies. Two solutions for the turbulent flow are found: one for infinite *local* Reynolds number which grows spatially as $x^{1/3}$; and another for small *local* Reynolds number which grows as $x^{1/2}$. Both solutions can be dependent on the upstream conditions. Also, the *local* Reynolds number diminishes with increasing downstream distance, so that even when the initial Reynolds number is large, the flow evolves downstream from one state to the other. Most of the available experimental data are at too low an initial Reynolds number and/or are measured too near the wake generator to provide evidence for the $x^{1/3}$ solution. New results, however, from a laboratory experiment on a disk wake and direct numerical simulations (DNS) are in excellent agreement with this solution, once the flow has had large enough downstream distance to evolve. Beyond this the ratio of turbulence intensity to centerline velocity deficit is constant, until the flow unlocks itself from this behavior when the *local* Reynolds number goes below about 500 and the viscous terms become important. When this happens the turbulence intensity ratio falls slowly until the $x^{1/2}$ region is reached. No experimental data are available far enough downstream to provide unambiguous evidence for the $x^{1/2}$ solution. The prediction that the flow should evolve into such a state, however, is confirmed by recent DNS results which reach the $x^{1/2}$ solution at about 200 000 momentum thicknesses downstream. After this the turbulence intensity ratio is again constant, until box-size affects the calculation and the energy decays exponentially. [DOI: 10.1063/1.1536976]

I. INTRODUCTION

The axisymmetric turbulent wake is a flow that has puzzled researchers for more than a half-century, since measured results have been either inconclusive or contradictive. In order to evaluate experimental data in the context of similarity analysis, a ''complete'' set of measured data is needed. Here, the term complete refers to the following necessary set of quantities: At least mean velocity and turbulence intensity distributions across the flow and the wake width. Figure 1 shows a sketch of the axisymmetric wake together with the coordinate system. U_∞ denotes the free stream velocity, $U_o = U_\infty - U_{CL}$ is the centerline velocity deficit, and δ is a measure of the wake width.

The axisymmetric wake is a challenging flow to measure because of the small velocity deficit, the slow decay of the velocity deficit downstream and a turbulence intensity of the same order as the deficit. In fact, the far axisymmetric wake still is at the threshold of what is possible to measure today using even the best wind tunnels and the most stable low-noise anemometer equipment. Also, unlike many other free shear flows for which the *local* Reynolds number remains constant or increases downstream, in the axisymmetric wake it drops slowly. Thus viscous effects continuously become more important until eventually they may dominate (if the flow extends far enough downstream). These varying viscous effects, together with the many very different possibilities for the structure of the near wake from different generators, considerably complicate interpretation of the data. The goal of this study is to use *equilibrium similarity theory* to sort out these different effects and isolate the regions in which they dominate or in which they can be ignored.

II. HISTORICAL REVIEW

The first complete set of data in the wake of an axisymmetric disk perpendicular to the flow was presented by Carmody,[1] who measured mean velocity, turbulence intensity, Reynolds stress and wake growth in an axisymmetric disk wake at a Reynolds number (R_D) of 70 000 where R_D is based on the free stream velocity and the disk diameter. Based on these measurements, the wake appeared to be self-similar 15 diameters from the disk, meaning that the mean velocity profiles appeared to collapse when normalized by the centerline deficit and a lateral length scale determined from the profile itself. The disk wake was also investigated

[a]Electronic address: peter.johansson@me.chalmers.se

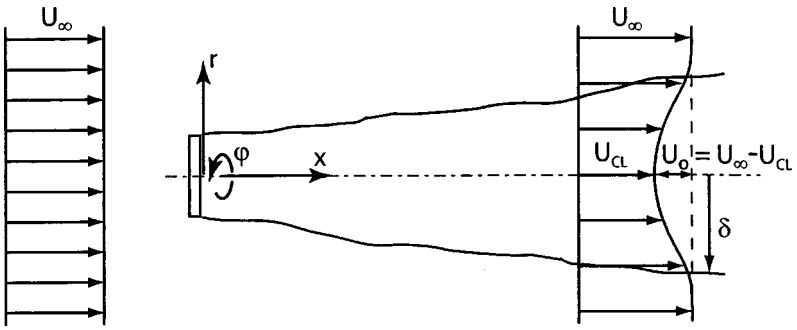

FIG. 1. Axisymmetric wake coordinates and definitions.

by Hwang and Baldwin,[2] who measured turbulence intensity and wake growth rate at up to 900 diameters downstream distance from the body. They did not, however, present centerline mean velocity decay. Both the Carmody[1] and Hwang and Baldwin[2] data show a significant scatter, presumably due to the limitations of the anemometers used at that time. Uberoi and Freymuth[3] measured the sphere wake at $R_D = 8600$ and stated that the wake achieved self-similar behavior at 50 diameters downstream, although they only measured a few more points farther downstream. Bevilaqua and Lykoudis[4] investigated the wakes of a sphere and a porous disk at $R_D = 10\,000$ with the same momentum deficit (drag), and reported that these became self-similar in terms of mean velocity and Reynolds stress profiles within ten diameters of the sphere and within twenty diameters of the porous disk—but not in the same manner; i.e., the sphere and the porous disk did not reach the same state of similarity. They concluded that this result was *not* consistent with the idea that the turbulence forgets how it was created, as commonly believed (cf. Townsend[5,6]).

A recent extensive experiment was reported by Cannon[7] who investigated the axisymmetric far wake behind five different wake generators (disk, sphere and three porous disks with varying porosity), all having the same drag and Reynolds number based on the momentum thickness of $R_\theta = U_\infty \theta / \nu \approx 3500$, where U_∞ is the free stream velocity, ν is the kinematic viscosity, and θ is the momentum thickness defined by

$$\theta^2 = \lim_{R\to\infty} \frac{1}{U_\infty^2} \int_0^R U(U_\infty - U) r\,dr. \tag{1}$$

This corresponds to values of R_D of 13 000 for the solid disk, 14 000–17 000 for the screens, and 21 500 for the sphere. The measurements extended over a range of x/θ from about 35 to 500. There were no conclusions about when the flow achieved self-similar behavior, and in fact it was not obvious that the turbulence intensities ever did.

During the last decade, researchers have primarily focused on the early development of the wake behind differently shaped axisymmetric bluff bodies; among them: İlday *et al.*,[8] Ostowari and Page,[9] Portiero and Perez-Villar,[10] and Sirviente and Patel.[11] All concluded that the wake became similar in *mean* velocity but the turbulence intensity profiles did not collapse. The initial evolution has also been studied numerically by Basu *et al.*,[12] who made a direct numerical simulation (DNS) of the axisymmetric wake for $R_D = 1500$. The authors claimed that the solution approached the self-similar state in a slow manner, but the computation was interrupted before this could be verified. From all the data referred to above, it is impossible to conclude whether the axisymmetric wake in general becomes self-similar at all; and if it does, when.

Very recently, Gourlay *et al.*,[13] presented the first DNS of the high Reynolds number ($R_D = 10\,000$) "late" wake (which can be directly compared with the "far" wake). The

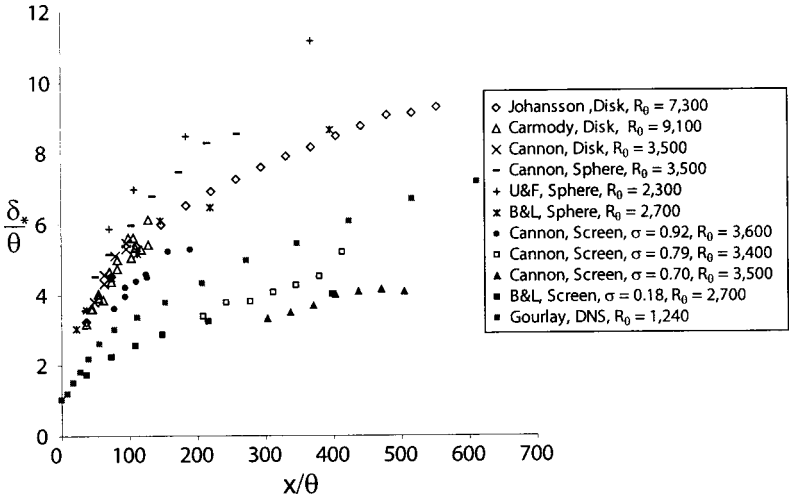

FIG. 2. Cross-stream length scale, δ_*/θ versus x/θ. For the screen wakes, the porosity, σ, is defined as σ = (solid area)/(total area).

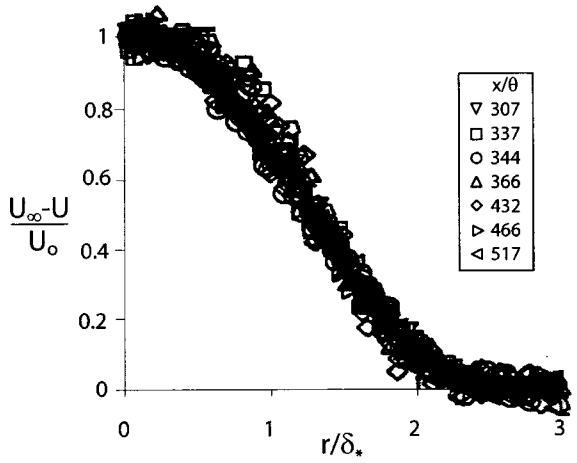

FIG. 3. Mean velocity profiles for the porous disk with $\sigma=0.70$, data from Cannon (Ref. 7).

simulation did not resolve a wake generator, but started from a Gaussian velocity profile consistent with a laminar wake (cf., Townsend[5,6] or Schlichting[14]) with superimposed random noise. The simulation ran to very large times, which corresponded to very large downstream distances, about $x/D\approx 4\times 10^5$ or $x/\theta\approx 3\times 10^6$! This is almost three orders of magnitude larger than any existing laboratory experiment. There was a brief comparison to the results of classical similarity analysis to check the reliability of the numerical data, but Gourlay *et al.*[13] did not make any statements about when or if the wake became self-similar.

Even more recently, the axisymmetric disk wake from $x/D=10$ to 60 was studied with the proper orthogonal decomposition (POD) technique by Johansson *et al.*[15] This work was extended to cover downstream distances up to $x/D=150$ by Johansson.[16,17] The latter provided mean velocity and streamwise velocity fluctuation profiles. These data, as well as those of Gourlay *et al.*[13] will be used extensively below.

The following observations can be made from all the investigations listed above:

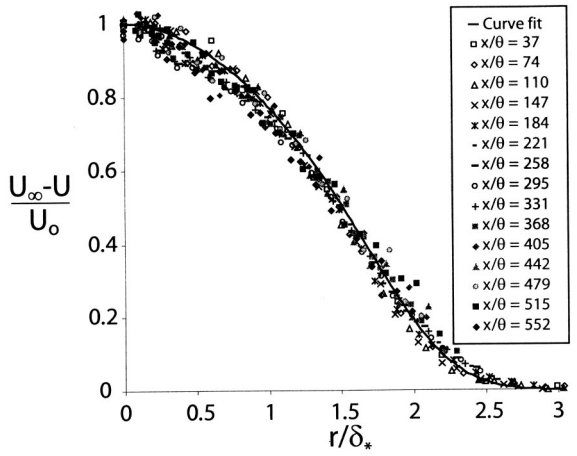

FIG. 4. Mean velocity profiles for disk, data from Johansson (Refs. 16 and 17). Solid line shows a curve fit according to Eq. (C7).

(i) Different initial conditions affect the growth rates, contrary to the classical theory which states that all wakes should depend only on the downstream distance, x, and the drag, $2\pi\rho U_\infty^2\theta^2$ (Townsend[5,6]). Here, ρ is the fluid density, U_∞ the free stream velocity, and θ the momentum thickness defined in Eq. (1). This is most strikingly illustrated by the flow visualization photographs of Cannon *et al.*[18]
Data from Carmody,[1] Uberoi and Freymuth,[3] Bevilaqua and Lykoudis,[4] Cannon,[7] Gourlay *et al.*,[13] and Johansson[16,17] are plotted in Fig. 2. (The data of Gourlay *et al.*[13] cover much larger x/θ than shown here, and will be discussed later.) These show the variation with x of the transverse length scale (wake width) defined by

$$\delta_*^2=\lim_{R\to\infty}\frac{1}{U_o}\int_0^R(U_\infty-U)r\,dr, \tag{2}$$

where U_o is the centerline velocity deficit. The data shown clearly do not collapse to a single curve independent of the wake generator. Note that the data by Bevilaqua and Lykoudis[4] are for two generators with the same drag, and that the data by Cannon[7] is for five generators with approximately the same drag. These source dependent effects do not seem to vanish, even for large Reynolds numbers or large downstream distance.

(ii) In apparent contradiction, the mean velocity profiles from all experiments collapse onto a single curve when scaled with centerline velocity deficit and δ_*, as illustrated in Figs. 3 and 4 for the data of Cannon[7] and Johansson,[16,17] respectively. The other references show just as good a collapse.

(iii) The turbulence intensity profiles presented by Carmody[1] and Cannon[7] do not collapse at all, even for fixed upstream conditions as shown in Fig. 5 for the data of Cannon[7] for the porous disk with $\sigma=0.70$. Here, very large downstream distances, up to $x/\theta>500$, are covered. By contrast, Fig. 6 shows profiles of $u'_{\max}/U_o$ for various downstream distances for the disk wake of Johansson.[16,17] Here, the turbulence intensity profiles seem to indeed collapse, but not before $x/\theta\approx 200$.

(iv) Finally, curve fits to the screen wake data by Cannon[7] indicate that square root and cube root downstream dependencies describe the wake growth equally well.

Clearly, there is much remaining to be explained. These issues cannot be reconciled simply by attributing them to measurement errors alone. Not all investigators could be incompetent, and in fact the internal consistency of the data suggests the opposite (e.g., momentum conservation, etc.) Nor are the problems presented by wake measurements more difficult than for grid turbulence for which hot-wire measurements have long been accepted.

The classical self-preservation approach to free shear flows was first questioned by George,[19,20] who argued that it was based on assumptions that were not in general valid. He proposed a new methodology called *equilibrium similarity*

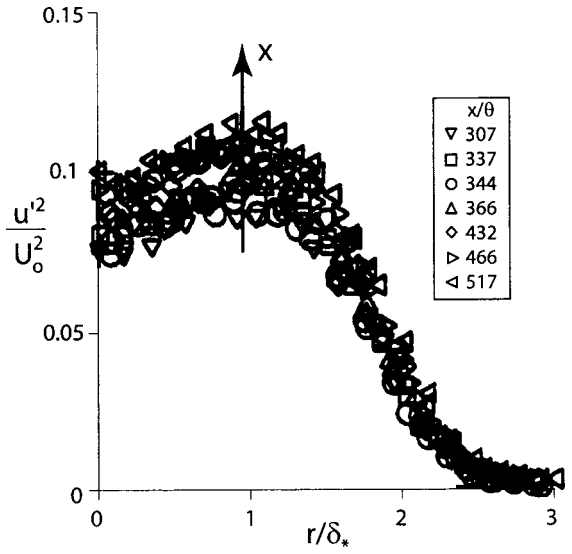

FIG. 5. Turbulence intensity profiles for the porous disk with $\sigma = 0.70$, data from Cannon (Ref. 7).

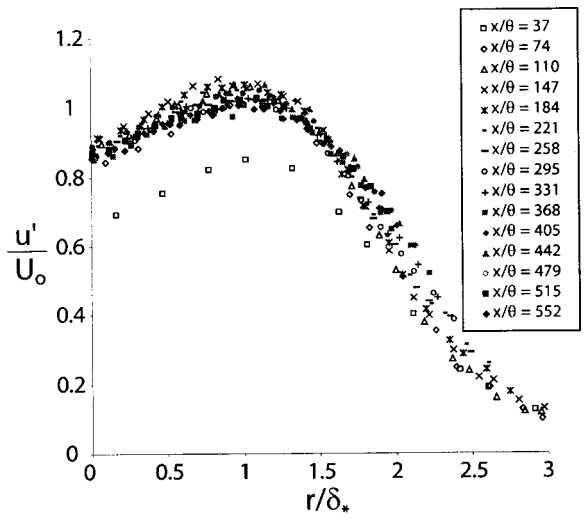

FIG. 6. Turbulence intensity profiles for disk, data from Johansson (Refs. 16 and 17).

analysis, and demonstrated with it that solutions were possible which depended *uniquely* on the upstream conditions. The new theory was in striking agreement with the nearly concurrent experiments of Wygnanski *et al.*[21] for two-dimensional wakes, which showed dramatic differences between spreading rates and eddy structure that depended on the wake generator.

George[19] also argued that the axisymmetric wake would behave similarly. He predicted that the mean velocity profiles from the different experiments would be the same, if scaled by the centerline deficit velocity and velocity deficit half-width, even if the wakes grew at different rates. This is consistent with the observations shown in Figs. 3 and 4. This result is very important, since previous researchers have often used the collapse of mean velocity profiles alone to argue that wakes are independent of upstream conditions. The whole point of George's analysis, however, is that *properly normalized mean velocity profiles always collapse*, and the *source-dependent differences only show up in the spreading rate and the higher turbulence moments*. This is clearly observed as noted above.

George[19] was unable to resolve whether the asymptotic axisymmetric wake would evolve as $\delta \sim x^{1/3}$ or as $\delta \sim x^{1/2}$. In fact, he showed from *ad hoc* assumptions about the dissipation that both solutions were consistent with the equations, depending on the Reynolds number. It did not appear to be possible, however, to decide which, if either, would be observed, or whether the flow would evolve from one to the other. Or even if such an evolution occurred, which would be observed first. As the careful experiments of Cannon[7] described earlier make clear, these questions are still very much in doubt.

In this paper, the analysis of George[19] is re-visited, corrected, and extended. It will be shown *without ad hoc* assumptions that two different equilibrium similarity solutions for the axisymmetric wake are indeed possible: One for very high *local* Reynolds numbers, and another for low. Most importantly, because the *local* Reynolds number *decreases* with distance downstream, the flow will be shown to eventually evolve from the high Reynolds number state to the lower, no matter how high the initial Reynolds number of the flow. And if the initial Reynolds number of the flow is too low, the high Reynolds number solution will not be observed at all. The available experimental and numerical data is analyzed, especially addressing the particular points listed above. Not surprisingly (given the state of confusion), most of the laboratory experiments are shown to take place in the evolution region. The direct numerical simulation of Gourlay *et al.*[13] is the only case where both the high and low local Reynolds number solution are found, since it is the only investigation that covers far enough downstream distances with high enough initial Reynolds number.

III. EQUILIBRIUM SIMILARITY ANALYSIS

The necessary equations to study are: the momentum equation, conservation of momentum, continuity, and the individual transport equations for Reynolds stresses in cylindrical coordinates. These are summarized in Appendix A, since they are not easily available in standard texts. In the spirit of George,[19,20] we seek solutions of the form (explicitly written here for the momentum equation and $\overline{u^2}$ equations, Eqs. (A1) and (A4), only—the others are treated similarly)

$$U - U_\infty = U_s(x) f(\eta, *), \quad -\overline{uv} = R_s(x) g(\eta, *), \tag{3a}$$

$$\frac{1}{2}\overline{u^2} = K_u(x) k_u(\eta, *), \quad \frac{1}{2}\overline{u^2 v} = T_{u^2 v} t_{u^2 v}(\eta, *), \tag{3b}$$

$$\overline{\frac{p}{\rho}\frac{\partial u}{\partial x}} = P_u(x) p_u(\eta, *), \quad \frac{1}{\rho}\overline{pu} = P_u^D(x) p_u^D(\eta, *), \tag{3c}$$

$$\varepsilon_u = D_u(x) d_u(\eta, *), \tag{3d}$$

where $\eta = r/\delta(x)$ and * denotes a possible (unknown) dependence on initial conditions. Note that two different sets of solutions will be found below, so the symbols will have dif-

ferent meanings depending on which is being discussed. Since each regime is discussed separately there should be no confusion.

For the particular type of ''equilibrium'' similarity solutions suggested in George,[20] *the terms in the governing equations must maintain the same relative balance as the flow evolves*. These ''equilibrium'' similarity solutions exist only if the terms within square brackets in Eqs. (B3)–(B8) have the same x-dependence, and are independent of the similarity variable, η. (Thus, the bracketed terms must remain proportional to each other as the flow evolves.) This is denoted by the symbol $\sim$ which should be interpreted as ''has the same x-dependence as.'' (Note that the symbol $\sim$ has nothing to do with ''order of magnitude'' in this paper.)

For the mean momentum equation of Eq. (B3), these equilibrium similarity constraints reduce to

$$\frac{\delta}{U_s}\frac{dU_s}{dx}\sim\frac{d\delta}{dx}\sim\frac{R_s}{U_\infty U_S}\sim\frac{v}{U_\infty\delta}. \tag{4}$$

There is nothing in the equations or the theory which suggests that the constants of proportionality are independent of source conditions, nor in fact do they appear to be. This is contrary to the usual assumptions in self-preservation analysis (cf., Townsend[5,6]). It is trivial to show that the relation between the first and second terms of Eq. (4) is satisfied by the momentum integral result of Eq. (B2).

The proper scale for $-\overline{uv}$ is obtained by using the second and third terms, which yields

$$R_s\sim U_\infty U_s\frac{d\delta}{dx}. \tag{5}$$

It is immediately obvious how the equilibrium similarity approach yields a different and more general result than the classical approach, where it is *assumed* without justification that $R_s=U_s^2$ (cf. Tennekes and Lumley[22]).

The same equilibrium similarity hypothesis can be applied to the component Reynolds stress equations; namely that all of the bracketed terms should remain proportional (i.e., have the same x-dependence). For example, inserting Eq. (3) into Eq. (A4) yields after some elementary calculus Eq. (B5). Thus equilibrium similarity can be maintained only if

$$\frac{\delta}{K_u}\frac{dK_u}{dx}\sim\frac{d\delta}{dx}\sim\frac{T_u\delta}{U_\infty K_u}\sim\frac{D_u\delta}{U_\infty K_u}\sim\frac{v}{U_\infty\delta}. \tag{6}$$

Similar relations arise from the other component equations, Eqs. (B6)–(B8).

All of these relations cannot simultaneously be satisfied given the constraints already placed on U_s, δ, and R_s from the mean momentum equation. A solution is possible, however, *if the viscosity is identically zero*, since then all terms involving the viscosity fall out of the problem. And also *a solution for finite viscosity is possible* if it can be shown that the production term, $-\overline{v^2}\partial(U-U_\infty)/\partial r$, in the Reynolds shear stress equation, Eq. (A7), is negligible relative to the leading terms.

It will be demonstrated below that these are in fact limiting solutions for very large *local* Reynolds number, and for very low *local* Reynolds number. Note that the latter solution should *not* be confused with the laminar solution, but instead identified with turbulent flow for which the velocity spectra do not have a developed $k^{-5/3}$ range (see George[20]). And by contrast, the high Reynolds number limit applies to a flow which has an easily apparent inertial subrange in the spectra. Further it will be demonstrated that no matter how high the Reynolds number of the drag-producing device, say $R_\theta=U_\infty\theta/v$, the diminishing *local* Reynolds number downstream will cause the equations (and the solutions as well) to slowly evolve from one regime to the other.

IV. THE INFINITE REYNOLDS NUMBER SOLUTION

A solution having the same x-variation as the classical solution can be derived by setting the viscous terms in Eqs. (B4)–(B8) exactly equal to zero, which corresponds to the limiting solutions at infinite Reynolds numbers. It is straightforward to show that all of the remaining constraints can be satisfied. Of particular interest are the following:

$$\frac{d\delta}{dx}\sim\frac{D_u\delta}{U_\infty K_u}, \tag{7}$$

$$K_u\sim K_v\sim K_w\sim U_s^2, \tag{8}$$

$$D_u\sim D_v\sim D_w\sim U_s^3/\delta. \tag{9}$$

Note that this is the solution obtained by George[19] by *assuming* the dissipation relation of Eq. (9). The scaling for the dissipation is just what one should expect for an infinite Reynolds number solution where the dissipation is completely controlled by the energetic turbulence (i.e., $\epsilon\propto u^3/l$ in the usual notation of texts).

It follows immediately after some manipulation that

$$\frac{\delta_*}{\theta}=a\left[\frac{x-x_o}{\theta}\right]^{1/3}, \tag{10}$$

$$\frac{U_s}{U_\infty}=b\left[\frac{x-x_o}{\theta}\right]^{-2/3}, \tag{11}$$

where $a=a(*)$, $b=b(*)$, and $x_o=x_o(*)$ is a virtual origin. This is, of course, the classical solution with but a single difference—the dependence of the coefficients on upstream conditions, *. This possible dependence must be acknowledged, since there is *nothing in the equations themselves* to suggest independence of upstream conditions. The mean velocity profile, on the other hand, can be shown to be independent of upstream conditions. This is achieved by incorporating a factor of $[R_s/(U_\infty U_s)d\delta/dx]$ into the definition of g so that there are no parameters at all in Eq. (B4), as noted by George.[19]

V. BOUNDS ON THE VALIDITY OF THE INFINITE REYNOLDS NUMBER SOLUTION

It was noted in the introduction that the cube root solutions simply do not account for most of the data, and especially the careful data of Cannon.[7] So where might the problem be? Firstly, even if the Reynolds number of the wake generator is high enough for the flow to be nearly inviscid, as

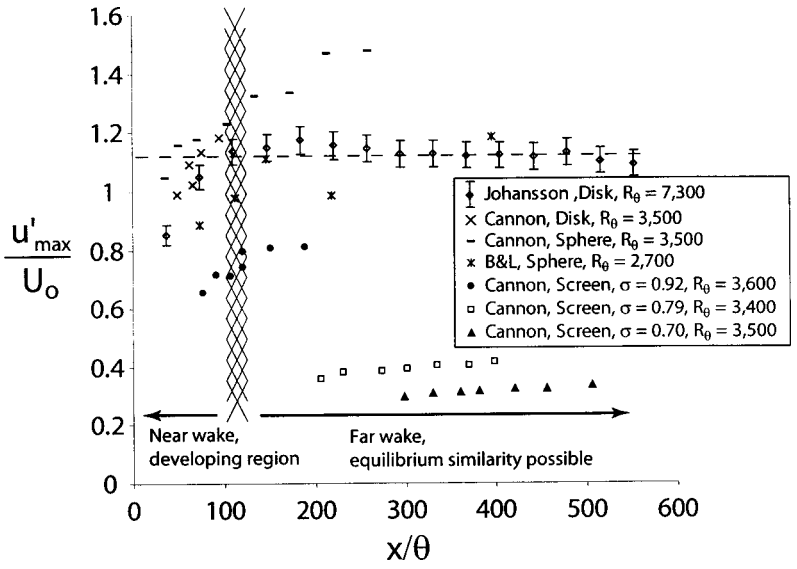

FIG. 7. Maximum turbulence intensities, data of Johansson (Refs. 16 and 17), Cannon, (Ref. 7), and Bevilaqua and Lykoudis (Ref. 4). Shaded area shows limit of near-wake transient for disk.

required for the similarity theory to be valid, it clearly can only apply after the transients from the wake generator have died off. Coincident with this, the turbulence intensity ratio, u'/U_s, must also reach a constant value, as demanded by Eq. (8) above. Note that appropriate choices for the similarity parameters K_u and U_s are $U_s=U_o$ and $K_u=u'^2_{\max}$, the centerline velocity deficit and maximum of the mean-square streamwise fluctuating velocities, respectively.

The ratio $u'_{\max}/U_o$ is plotted in Fig. 7 versus x/θ for the data of Johansson,[16,17] Bevilaqua and Lykoudis,[4] and Cannon.[7] There is a large uncertainty as to whether the data of Bevilaqua and Lykoudis[4] and Cannon[7] reach a horizontal line. Note that the data of Cannon[7] for the screen with $\sigma=0.70$ is based on Fig. 5 and the data of Johansson[16,17] are obtained from Fig. 6. The data from Johansson[16,17] tends to fall onto a line, at least after $x/\theta\approx120$. The error bars indicate an uncertainty in the data of 4%. This error originates primarily in the difficulty of estimating the centerline mean velocity difference, since the mean velocity data is affected by drift in the anemometer calibration. This is discussed in detail in Johansson.[16,17] There is no doubt, however, that the flow is still developing until at least $x/\theta=120$ ($x/D\approx30$), beyond which it appears to have settled in to an equilibrium similarity state.

This conclusion can be compared to the findings of the POD studies of Johansson *et al.*[15,23] (see also George *et al.*[24]), who showed that the POD modal distribution was changing until $x/D\approx50$ ($x/\theta\approx184$). The energy distribution went from an azimuthal mode 1 dominance at $x/D=10$ to an azimuthal mode 2 dominance by $x/D=50$, with both modes being equally important at $x/D=30$. Beyond $x/D=50$, the decomposition hardly changed at all. By contrast the turbulence intensity seems to have settled in by $x/D\approx30$ ($x/\theta\approx120$), but the overshoot between $x/\theta\approx120$ and 200 may be significant. Other quantities, such as the growth rate must be taken into account before specifying the exact location of the start of the equilibrium similarity range. Uberoi and Freymuth[3] concluded that their sphere wake became self-similar after $x/D=50$ (corresponding to $x/\theta\approx300$ in their case). Given the difference in initial conditions, there are no particular reasons that the these two flows should develop in exactly the same way, either initially or far downstream.

It is easy to show that, unlike most other free shear flows, this infinite Reynolds number solution contains the seeds of its own destruction. The product of $U_\infty\delta_*/\nu$ and $d\delta_*/dx$ controls the relative importance of the neglected viscous terms in the mean momentum [Eq. (B4)] and Reynolds shear stress equations [Eqs. (B5)–(B8)]. This product can be simply related to the *local* Reynolds number, $R=U_s\delta_*/\nu$, by substituting Eqs. (10) and (11) into the definitions to obtain

$$\frac{U_\infty\delta_*}{\nu}\frac{d\delta_*}{dx}=\frac{a^2}{3}\frac{U_\infty\theta}{\nu}\left[\frac{x-x_o}{\theta}\right]^{-1/3}=\frac{a}{3b}R, \tag{12}$$

where

$$R=\frac{U_s\delta_*}{\nu}=abR_\theta\left[\frac{x-x_o}{\theta}\right]^{-1/3}. \tag{13}$$

Thus, no matter how large the initial Reynolds number, R_θ, eventually far enough downstream the *local* Reynolds number, R, is diminished until the viscous terms can no longer be neglected. And if the viscous terms are not negligible, then the infinite Reynolds number similarity solution cannot be even approximately true. This is illustrated in Fig. 8, using the data of Johansson,[16,17] Carmody,[1] Cannon,[7] Uberoi and Freymuth,[3] Bevilaqua and Lykoudis,[4] and Gourlay *et al.*[13] Clearly the local Reynolds numbers in the experiments drops drastically as the flow evolves downstream, so eventually the viscous terms become important, even if initially negligible.

The effects of the changing *local* Reynolds number, R, can also be clearly seen in the one-dimensional velocity spectra of Uberoi and Freymuth[3] and Gourlay *et al.*[13] shown in Fig. 9. As noted by George,[20] high Reynolds number solutions apply only if there is a clear inertial subrange in the power spectrum. This insures that the energy and Reynolds stress scales of motion are effectively inviscid. For R greater than 1600, this is clearly the case, with about two decades of

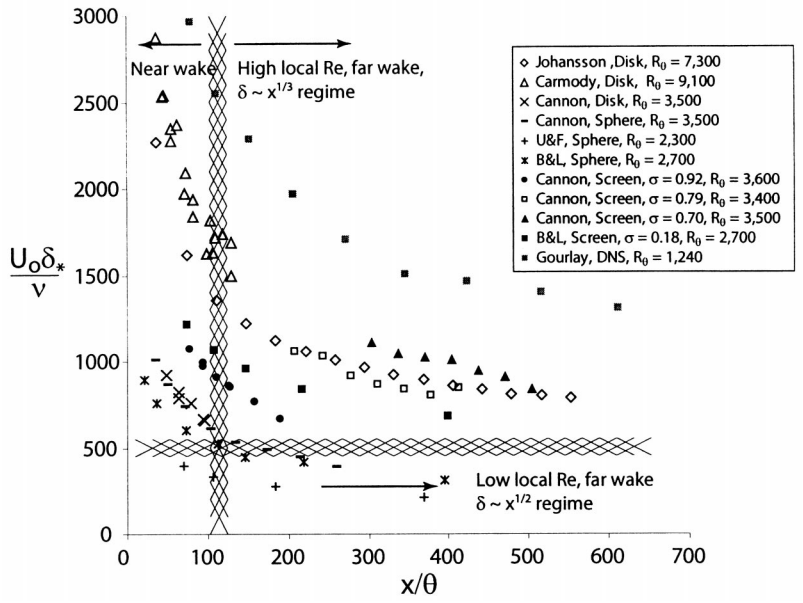

FIG. 8. Local Reynolds number. Shaded areas show lower limit for high Reynolds number solution and limit of near-wake transient for disk.

inertial subrange. By $R=400$, the existence of an inertial subrange is questionable, and by $R=200$ it is clearly gone.

The approximate lower limit for the high Reynolds number solution of $R\approx 500$ is indicated on Fig. 8 by the horizontal shaded line. None of the data below this line satisfy the conditions for the high Reynolds number solution. Also shown in Fig. 8 by the vertical shaded line is the approximate boundary of the transient (or near wake) region for the disk as described above. Clearly most of the experimental data do not satisfy the conditions for the high Reynolds number solution to apply. Before examining in detail the experiments that do, the low Reynolds number solution will be developed below.

VI. THE LOW RE SOLUTION

As noted above (and by George[19]), there is another equilibrium similarity solution to the same set of equations. The difference is that this time all the terms involving viscosity are kept in both the mean and Reynolds shear stress equations. This produces one additional constraint of the mean momentum equation [Eq. (B4)]

$$\frac{d\delta}{dx}\sim\frac{\nu}{U_\infty\delta}. \tag{14}$$

It is extremely important to note that even though some of the relations are the same (e.g., $K_u/U_s^2=$constant), the constants of proportionality (or more properly, the parameters of proportionality since they all depend on *, the unknown details of the initial conditions) are most likely different from those governing the infinite Reynolds number solution.

There is one problem which at first glance appears to be quite serious. All of the constraints in the Reynolds shear stress equation cannot be met, in particular the one arising from the production term, $\overline{v^2}\partial(U-U_\infty)/\partial r$. This offending term dies off with distance downstream faster than the remaining terms in the equation, in fact as $x^{-7/2}$ compared to $x^{-5/2}$ for the rest. Therefore, it can also be neglected in the analysis since it does not survive asymptotically (exactly like the Reynolds stress convection terms in the outer boundary layer analysis of George and Castillo[25]). But since the difference in decay as $x^{-7/2}$ and $x^{-5/2}$ is very small, it clearly will take a considerable distance downstream to reach this new state of equilibrium. Moreover, this new state will be very difficult to recognize from δ_* and U_o alone.

It is straightforward to show that Eq. (14) can be integrated to obtain

$$\frac{\delta_*}{\theta}=c\ \ R_\theta^{-1/2}\left[\frac{x-x_{oo}}{\theta}\right]^{1/2}, \tag{15}$$

$$\frac{U_s}{U_\infty}=d\ \ R_\theta\left[\frac{x-x_{oo}}{\theta}\right]^{-1}, \tag{16}$$

where as before $c=c(*)$, $d=d(*)$, and $x_{oo}=x_{oo}(*)$ is a virtual origin which most likely is different than the one obtained above. Unlike the infinite Reynolds number solutions, the mean velocity profile cannot be shown to be independent of upstream conditions because of the additional term in the momentum equation. Note that the mean profile is not the same as for the high *local* Reynolds number wake, at least in principle, because it is a solution to different equations involving viscosity. (See, for example, Fig. 15 and Appendix C.)

It is easy to show that the local Reynolds number continues to fall with increasing distance downstream; therefore, the approximations improve with distance downstream. Moreover, since the viscous stresses and Reynolds stresses both decay as $x^{-3/2}$, the flow will remain a low *local* Reynolds number turbulent wake forever.

An important clue as to if and when this low Reynolds number solution regime applies is the constancy of the ratio, K_u/U_s^2, or in the data the constancy of the ratio $u'_{\max}/U_o$. This is exactly the same condition applied above to identify the high Reynolds number region; so if the constant is the same for both high and low Reynolds number solutions, it will be extraordinarily difficult to tell them apart since they

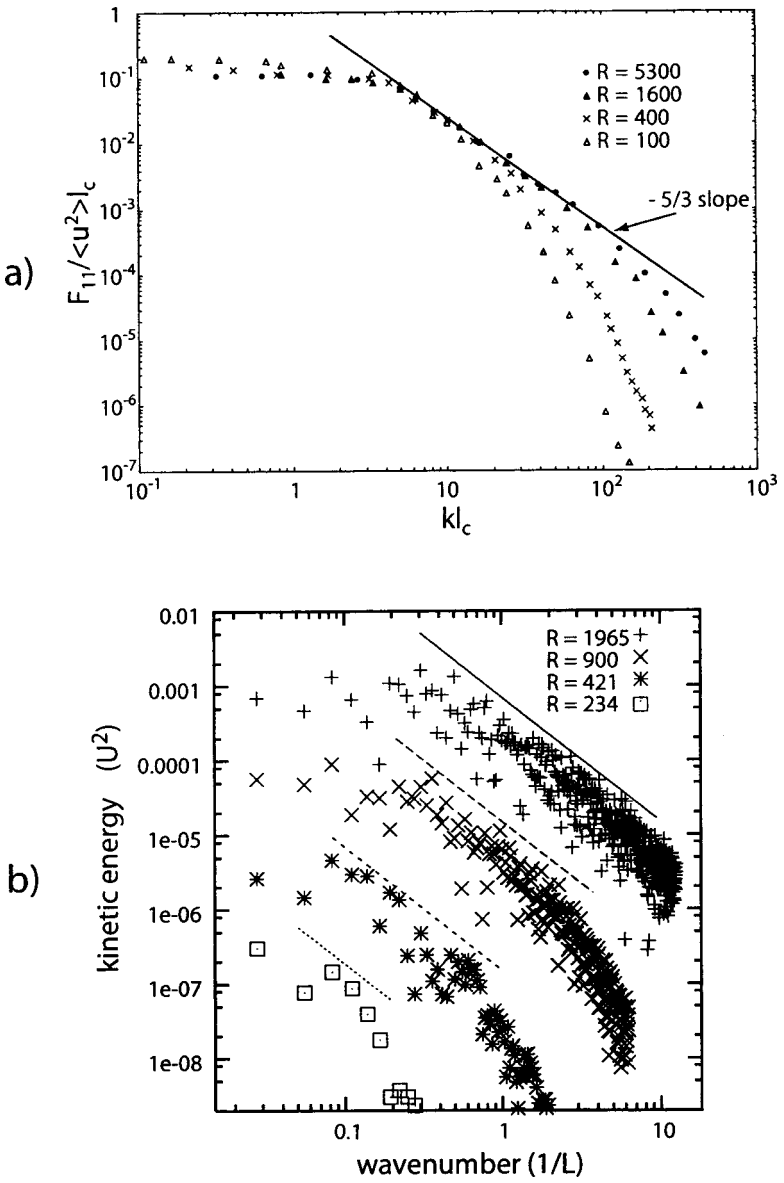

FIG. 9. Dependence of the spectra on *local* Reynolds number. (a) Data of Uberoi and Freymuth (Ref. 3) [$l_c = D^{2/3}(x-x_o)^{-2/3}$, $x_o = 12D$]. (b) Data of Gourlay *et al.* (Ref. 13). Lines indicate $k^{-5/3}$ slopes.

differ by only $x^{1/2}/x^{1/3}$. Fortunately, the intensity ratios appear to differ significantly as will be seen below, so it is quite easy to decide where the infinite Reynolds number region ends and where the viscous one begins, at least for the Gourlay *et al.*[13] data.

VII. IDENTIFICATION OF THE DIFFERENT REGIMES FROM DATA

A necessary condition for any data to be considered is that momentum is conserved. For the near wake this requires inclusion of the nonlinear term in Eq. (1); but for all positions of interest here, momentum conservation reduces to

$$U_o \delta_*^2 = U_\infty \theta^2. \tag{17}$$

All of the experimental data appear to satisfy this requirement, as does the DNS data of Gourlay for $x/\theta > 500$. Moreover, as noted above, for similarity to be valid the ratio $u'_{\max}/U_o$ has to be constant. The constant may be, in principle at least, different for the high and low Reynolds number regions. In fact, it is the constancy or lack of constancy of $u'_{\max}/U_o$ that most easily identifies the various similarity solution regimes.

As noted above, only a few of the many sets of experimental data actually satisfy the conditions for the infinite Reynolds number solution to apply. Only the experimental data of Johansson[16,17] and the DNS data of Gourlay[13] will be considered further here. Of these, only the DNS data completes the evolution to the low Reynolds number solution.

A. A high Reynolds number experiment

The Johansson data were taken in the MTL tunnel of the Swedish Royal Institute (KTH), Stockholm using rakes of 15 hot-wires. The disk was 20 mm in diameter and the flow speed was 20.4 m/s, corresponding to $Re_\theta = 7300$. The 7 m long test section and very low background turbulence intensity permitted measurements downstream to $x/D = 150$, or $x/\theta = 552$. The experiment is described in detail in Johansson.[16,17] The mean velocity and turbulence intensity

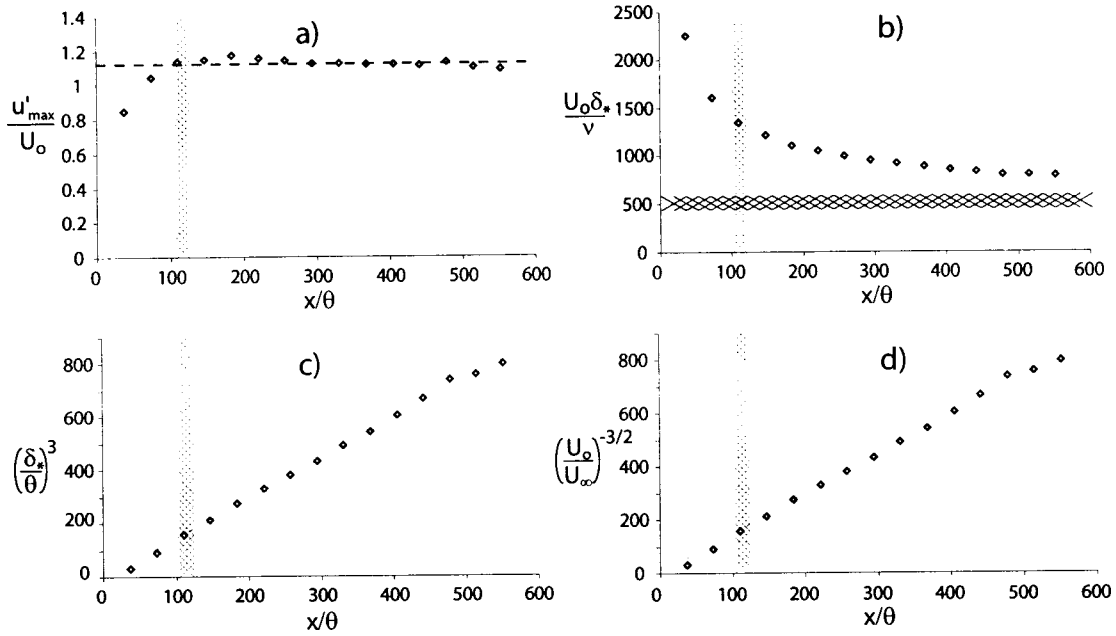

FIG. 10. (a) Maximum turbulence intensity, (b) local Reynolds number, (c) wake width, and (d) velocity deficit. Data of Johansson (Refs. 16 and 17). Shaded areas show lower limit for high Reynolds number solution and limit of near-wake transient.

profiles have already been shown in Figs. 4 and 6, respectively. Figure 10 summarizes all the remaining important parameters mentioned above for the full picture of the high *local* Reynolds number similarity region for the disk wake.

The turbulence intensity normalized by the velocity deficit at the centerline is constant beyond $x/\theta \approx 120$. The *local* Reynolds number is above 500, even at the farthermost downstream position. The plot of $(\delta_*/\theta)^3$ versus x/θ is linear, as is the plot of $(U_c/U_o)^{-3/2}$, exactly as required by the high Reynolds number similarity results of Eqs. (10) and (11), respectively. Linear regression yields values for the constants as: $a=1.14$, $b=0.77$, $x_o=-2.4\theta$.

B. Recent high Reynolds number DNS

The DNS data of Gourlay *et al.*[13] cover very large downstream distances as mentioned in the introduction, and both the high and low Reynolds number regimes can be observed. The original data were presented as a function of nondimensionalized time, tU/L, where the reference velocity $U=1$ and reference length $L=1$. When converting to downstream distance, x/θ, it was first assumed that $tU=x$, and the velocity profiles were then integrated according to Eq. (1). All results presented here are plotted versus x/θ to facilitate comparison with the experimental data.

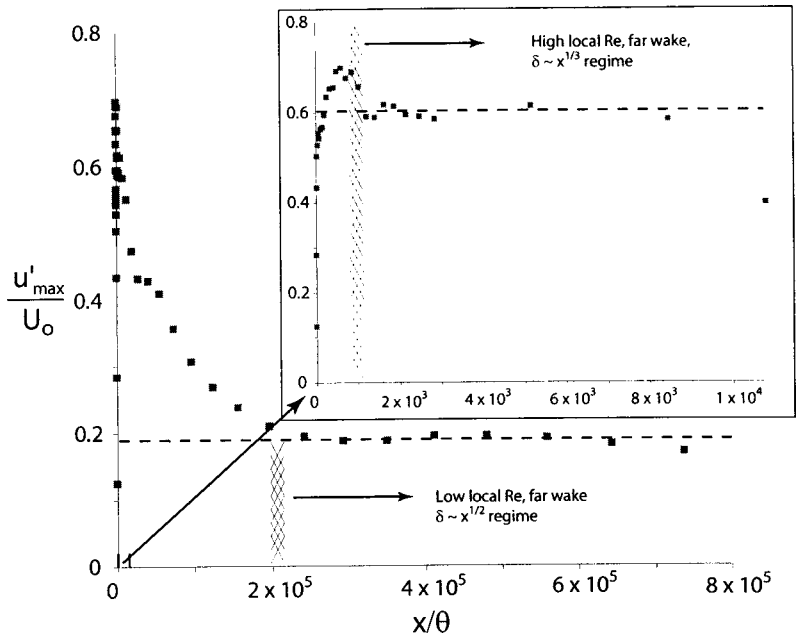

FIG. 11. Maximum turbulence intensities, data of Gourlay *et al.* (Ref. 13). Inset shows the region $0 \leqslant x/\theta \leqslant 10^4$. Shaded area shows limit of near-wake transient.

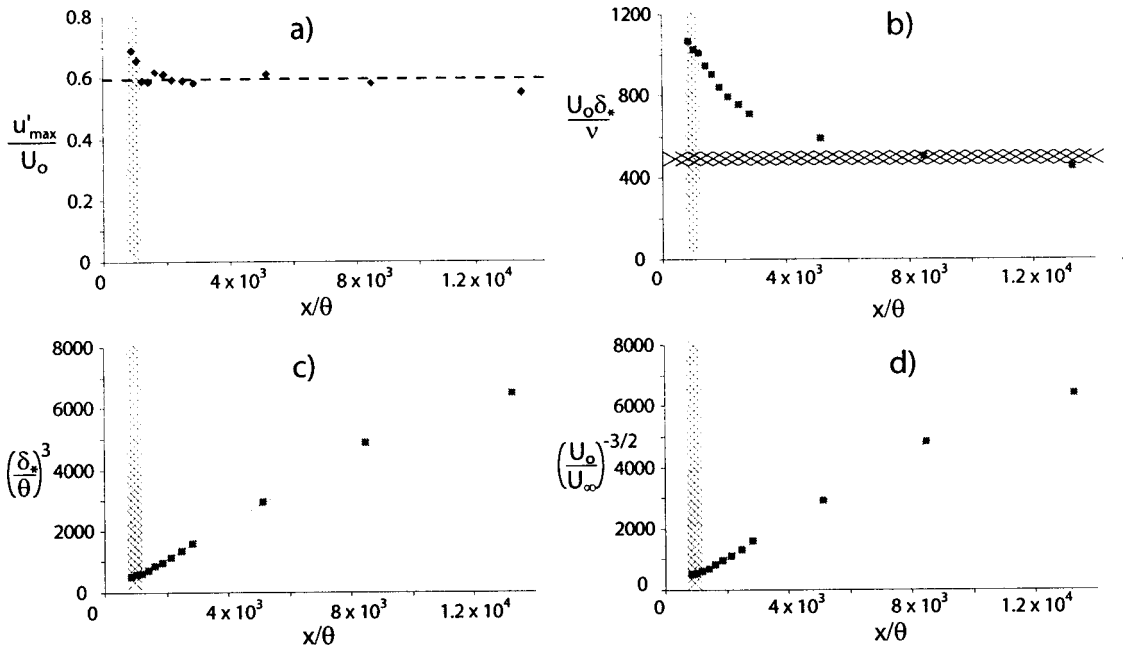

FIG. 12. (a) Maximum turbulence intensity, (b) *local* Reynolds number, (c) wake width, and (d) velocity deficit. Data of Gourlay *et al.* (Ref. 13). Shaded areas show lower limit for high Reynolds number solution and limit of near-wake transient.

In Fig. 11, the turbulence intensities of Gourlay *et al.*[13] are shown. Two regions of constant normalized turbulence intensity can be observed: One for $1000<x/\theta<8\,000$ approximately (see inset), and the other for $200\,000<x/\theta<600\,000$ approximately. This wake clearly reaches the first equilibrium similarity region much farther downstream than the disk wake of Johansson[16,17] considered above. This might be related to the level of turbulence intensity which is much lower (almost a factor of two) than the disk wake results. (Note that the turbulence intensity is even lower for the porous screens of Cannon[7] shown in Fig. 7.) Because of the low turbulence intensity of these flows, it is possible it takes such large downstream distances for the flow to reach equilibrium because the time scale of the energy-containing eddies, δ_*/u', is correspondingly increased. Figure 12 summarizes the important parameter variation for the first region identified above.

The turbulence intensity normalized by the centerline velocity deficit begins to drop slowly after $x/\theta\approx8000$, which is about where the local Reynolds number has reached the previously suggested threshold of 500. Clearly, this region should be identified with the high Reynolds number solution. As for the disk data, $(\delta_*/\theta)^3$ and $(U_o/U_\infty)^{-3/2}$ are both linear over the same range for which the intensity ratio is constant, and begin to deviate about when the intensity ratio begins to drop and the Reynolds number drops below the threshold value. Regression fits of Eqs. (10) and (11) yield values for the constants of: $a=0.84$, $b=1.44$, and $x_o=200\theta$. These are quite different from the values above for

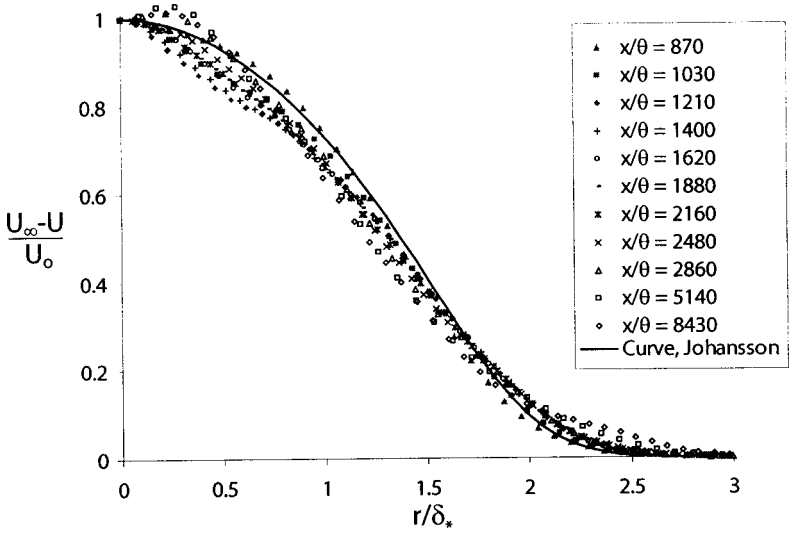

FIG. 13. Mean velocity profiles, near wake data of Gourlay *et al.* (Ref. 13). Solid line shows the fit according to Eq. (C7) to the data of Johansson (Refs. 16 and 17) shown in Fig. 4.

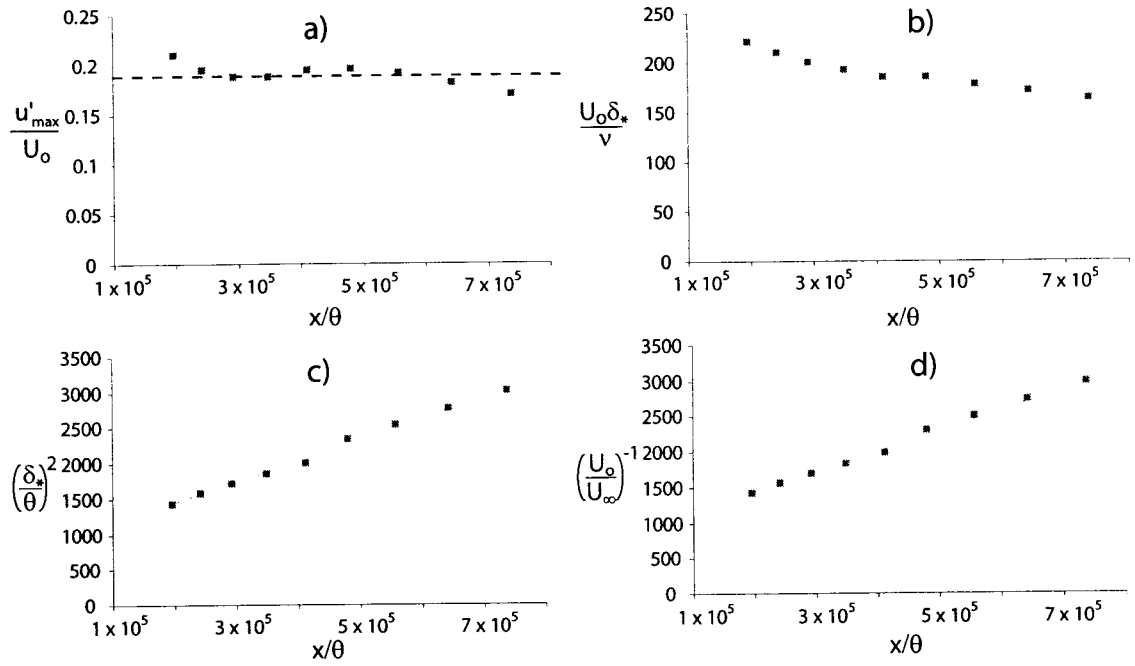

FIG. 14. (a) Maximum turbulence intensity, (b) *local* Reynolds number, (c) wake width, and (d) velocity deficit. Data of Gourlay *et al.* (Ref. 13).

the disk wake, making clear the effect of different initial conditions.

Figure 13 shows the normalized mean velocity deficit profiles for this portion of the Gourlay data. Also shown on the plot is the best fit line to the mean velocity deficit data of Johansson shown in Fig. 4. These should be exactly the same according to the similarity theory, since any differences should show up only in the growth rate and the magnitude of the Reynolds stress; and they are, but only at $x/\theta=1030$. The differences may be due to the scatter in the DNS data because of the limited statistical sample. Note that the DNS data are not averaged over time, but instead spatially (see Gourlay *et al.*[13]). Alternatively, perhaps the mean velocity profile is affected somewhat earlier than the turbulence intensity ratio by the lower local Reynolds number of the DNS data. Or perhaps simply the curve fit of Fig. 4 should be slightly altered.

The low local Reynolds number similarity region can only identified in the DNS data of Gourlay *et al.*,[13] the second region of constant intensity ratio identified above. The important parameters are shown in Fig. 14. The local Reynolds number is well below the threshold for the high Reynolds number solution to be valid, so clearly the low Reynolds number solution is appropriate. Thus it is not surprising that the plots of $(\delta_*/\theta)^2$ and $(U_o/U_\infty)^{-1}$ are remarkably linear. Regressive fits of Eqs. (15) and (16) yield values for the constants of $c=1.90$, $d=0.28$, $x_{oo}=-3.0\times10^5\theta$. Note that the high value for the virtual origin is consistent with the fact that this region does not begin until $\delta_*/\theta\approx33$! In fact, instead of a virtual origin, it might be more appropriate to think of it as a starting value for δ_*/θ when the low Reynolds number equilibrium similarity region begins.

Figure 15 shows the normalized mean velocity deficit profiles for $1.96\times10^5\leqslant x/\theta\leqslant8.41\times10^5$. The collapse is remarkable. Also shown is the curve fit to the high Reynolds number Johansson data. Clearly these are different, consistent with the fact that the mean momentum equation is different because of the presence of the viscous stress. Also shown, overlaying the data almost perfectly is the exponential eddy viscosity profile developed in Appendix C. Note that this is not the same as the laminar solution: First because the ''turbulent viscosity'' is about 15 times the fluid viscosity; second, the turbulence intensity ratio is nonzero and plays a significant role in the flow evolution.

Finally, Fig. 16 shows a linear-linear plot of the Gourlay data for all values of x/θ. Also shown are the curve fits discussed above for the high and low Reynolds number regimes. The figure makes clear how truly far downstream these DNS data really go, and also what a small portion of the total is the truly high Reynolds number part of it. It is also clear why, in the absence of the theory developed herein, previous experimenters have had such difficulty making sense of their data.

C. Summary of data analysis

Based on the results of the similarity theory stated above, the evolution of the axisymmetric wake flow can be described as follows:

(i) In the vicinity of the wake generator, the ''near wake'' region, the flow does not obey the equations governing the equilibrium similarity state presented in Appendix A. In other words, the flow is in nonequilibrium.

(ii) Given the time (or downstream distance) to adjust, the assumptions underlying the equilibrium similarity solutions are satisfied. When the flow has reached the ''far wake'' region, characterized by the ratio $\sqrt{u^2}/U_o$ being constant, and provided that the initial local Rey-

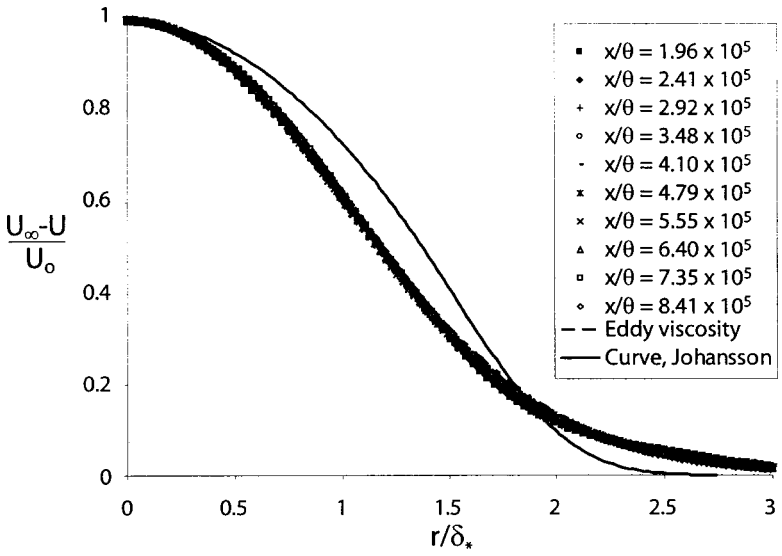

FIG. 15. Mean velocity profiles, far wake data of Gourlay *et al.* (Ref. 13). Dashed line shows the solution to the eddy viscosity model, Eq. (C4). Solid line shows the fit according to Eq. (C7) to the data of Johansson (Refs. 16 and 17) shown in Fig. 4.

nolds number, $R=U_o\delta_*/v$ (that decreases downstream), is still is large enough, the flow will behave like it is in equilibrium with $\delta_*\sim x^{1/3}$, and $U_o\sim x^{-2/3}$. For the disk wake of Johansson,[16,17] this was found to happen when $x/\theta\approx 120$. For the DNS simulation of Gourlay *et al.*[13] this was true after about $x/\theta\approx 1000$.

(iii) When the local Reynolds number, R, drops below a threshold value, the flow is forced from its equilibrium similarity state by the leading order viscous term. Most notable is that the ratio $\sqrt{u^2}/U_o$ begins to decrease. This slow decrease continues for an extremely long distance downstream. The threshold value of R for the beginning of this decline is seen to be about 500, consistent with the disappearance of the inertial subrange in the spectrum noted earlier.

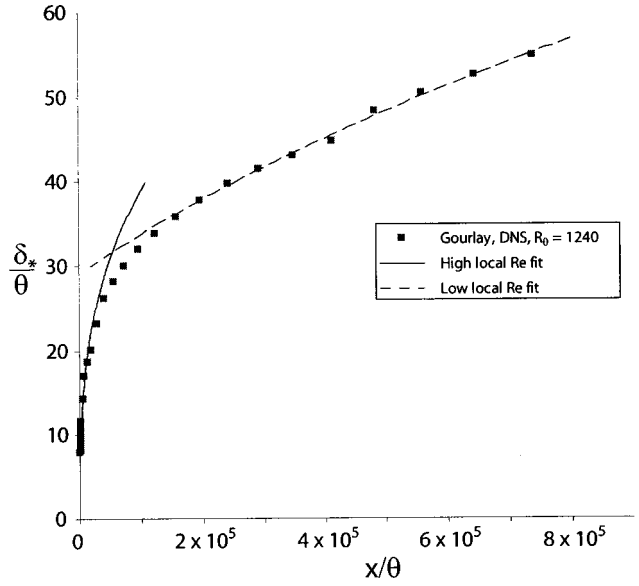

FIG. 16. Cross-stream length scale, δ_*/θ versus x/θ, data of Gourlay *et al.* (Ref. 13).

(iv) After sufficient time, the flow readjusts into a different equilibrium state, with different governing equations including the leading order viscous term. Here, $\sqrt{u^2}/U_o$ is again constant, and the wake width now grows like $\delta_*\sim x^{1/2}$, and the velocity deficit decays like $U_o\sim x^{-1}$. This region was only found in the DNS simulation of Gourlay *et al.*[13] at about $x/\theta\approx 2\times 10^5$.

(v) After $x/\theta\approx 5\times 10^5$, the turbulence intensity drops again, and seems to decay exponentially. This is a behavior found in other simulations when the computational or experimental box-size is too small (e.g., by Moser *et al.*[26] and George and Wang[27]). Shortly thereafter, the momentum integral ceases to be constant.

VIII. CONCLUSIONS

Equilibrium similarity considerations can be applied to the axisymmetric turbulent wake, without the arbitrary assumptions of earlier theoretical studies. Two solutions for the turbulent flow are found: One for infinite local Reynolds number which grows spatially as $x^{1/3}$; and another for small local Reynolds number, which grows as $x^{1/2}$. Both solutions depend on the upstream conditions. For both solutions, the local Reynolds number of the flow diminishes with increasing downstream distance. As a consequence, even when the initial Reynolds number is large, the flow evolves downstream from the high to the low Reynolds number state.

Most of the available experimental data were at too low an initial Reynolds number and/or were measured too close to the wake generator to provide evidence for the $x^{1/3}$ solution. New results, however, from a laboratory experiment on a disk wake and DNS are in excellent agreement with this solution, once the flow has had large enough downstream distance to evolve. Beyond this, the ratio of turbulence intensity to centerline velocity deficit is constant until the flow unlocks itself from this behavior when the local Reynolds number goes below about 500. When this happens the turbulence intensity ratio falls slowly until the $x^{1/2}$ region is reached at approximately $R=220$. This contrary to previous

assumptions that the high Reynolds number wake always appears far downstream and remains until the local Reynolds number is of order unity (cf. Tennekes and Lumley[22]).

No experimental data is available far enough downstream to provide evidence for the $x^{1/2}$ solution. The prediction that the flow should evolve into such a state, however, is confirmed by recent direct-numerical simulation (DNS) results which reach the $x^{1/2}$ at about 200 000 momentum thicknesses downstream, after which the turbulence intensity ratio is again constant until box-size affects the calculation.

The primary conclusion of this paper is that initial conditions and local Reynolds number effects dominate the axisymmetric wake. Thus previous speculations that near wake effects persist far downstream are correct. Moreover, contrary to popular belief, this asymptotic dependence on upstream conditions is consistent with a proper equilibrium similarity analysis. The effect of initial conditions does not, however, show up in the normalized velocity profiles, but in the growth rate and the higher velocity moments, exactly as the theory predicts.

ACKNOWLEDGMENTS

Earlier versions of this work was presented as a poster (P.B.V.J. and W.K.G.[28]) at the IUTAM symposium on Bluff Body Wakes and Vortex-Induced Vibrations (BBVIV-2) in Marseille, France, 2000, and as a conference paper (P.B.V.J. and W.K.G.[29]) at the Second International Symposium on Turbulence and Shear Flow Phenomena (TSFPII) in Stockholm, Sweden, 2001. It was initially supported by Chalmers University of Technology. It continues with the support of the Swedish Research Council, Grant No. 2641.

APPENDIX A: GOVERNING EQUATIONS

The Reynolds averaged x-momentum equation for the axisymmetric far wake without swirl reduces to second order to

$$U_\infty \frac{\partial}{\partial x}(U-U_\infty) = -\frac{1}{r}\frac{\partial}{\partial r}(r\overline{uv}) + \upsilon \frac{1}{r}\frac{\partial}{\partial r}\left(r\frac{\partial}{\partial r}(U-U_\infty)\right). \tag{A1}$$

Here, uppercase letters denote averaged quantities and lowercase letters represent the fluctuating part. A bar over the quantity denotes an ensemble average. The viscous term is usually neglected, but retained here.

The momentum equation can be integrated over a cross section to yield an integral constraint for the conservation of momentum

$$U_\infty \int_0^\infty (U_\infty - U) r\,dr \cong \theta^2 U_\infty^2, \tag{A2}$$

where θ is the momentum thickness.

The equation of continuity for the mean and fluctuating part of the velocities are

$$\frac{\partial U}{\partial x} + \frac{1}{r}\frac{\partial}{\partial r}(rV) = 0, \quad \frac{\partial u}{\partial x} + \frac{1}{r}\frac{\partial}{\partial r}(rv) + \frac{1}{r}\frac{\partial w}{\partial \varphi} = 0. \tag{A3}$$

As noted by George,[20] the momentum and continuity equations alone are not sufficient to determine the similarity constraints. Even the inclusion of the kinetic energy equation is not enough to close the system so that the x-dependence can be determined. Instead, the individual Reynolds stress equations have to be investigated. These, together with the constraint of continuity on the pressure-strain rate terms, provide the necessary conditions. The component Reynolds stress equations for the far wake are

$\overline{u^2}$ balance

$$U_\infty \frac{\partial}{\partial x}\left(\frac{1}{2}\overline{u^2}\right) = -\overline{uv}\frac{\partial}{\partial r}(U-U_\infty) - \frac{1}{r}\frac{\partial}{\partial r}\left(r\frac{1}{2}\overline{u^2 v}\right) + \overline{\frac{p}{\rho}\frac{\partial u}{\partial x}} - \frac{1}{\rho}\frac{\partial}{\partial x}\overline{pu} + \upsilon\frac{1}{r}\frac{\partial}{\partial r}\left\{r\frac{\partial}{\partial r}\left(\frac{1}{2}\overline{u^2}\right)\right\} - \varepsilon_u, \tag{A4}$$

$\overline{v^2}$ balance

$$U_\infty \frac{\partial}{\partial x}\left(\frac{1}{2}\overline{v^2}\right) = -\frac{1}{r}\frac{\partial}{\partial r}\left(r\frac{1}{2}\overline{v^3}\right) + \overline{\frac{vw^2}{r}} + \frac{1}{r}\overline{\frac{p}{\rho}\frac{\partial rv}{\partial r}} - \frac{1}{r}\frac{1}{\rho}\frac{\partial}{\partial r}\overline{rpv} + \upsilon\frac{\partial}{\partial r}\left\{\frac{1}{r}\frac{\partial}{\partial r}\left(r\frac{1}{2}\overline{v^2}\right)\right\} - \varepsilon_v, \tag{A5}$$

$\overline{w^2}$ balance

$$U_\infty \frac{\partial}{\partial x}\left(\frac{1}{2}\overline{w^2}\right) = -\frac{1}{r}\frac{\partial}{\partial r}\left(r\frac{1}{2}\overline{uw^2}\right) - \overline{\frac{vw^2}{r}} + \overline{\frac{p}{\rho}\frac{1}{r}\frac{\partial w}{\partial \varphi}} + \upsilon\frac{\partial}{\partial r}\left\{\frac{1}{r}\frac{\partial}{\partial r}\left(r\frac{1}{2}\overline{w^2}\right)\right\} - \varepsilon_w, \tag{A6}$$

$\overline{uv}$ balance

$$U_\infty \frac{\partial}{\partial x}(\overline{uv}) = -\overline{v^2}\frac{\partial}{\partial r}(U-U_\infty) - \frac{1}{r}\frac{\partial}{\partial r}(r\overline{uv^2}) + \frac{\overline{uw^2}}{r} + \overline{\frac{p}{\rho}\left(\frac{\partial u}{\partial r}+\frac{\partial v}{\partial x}\right)} - \frac{1}{\rho}\left(\frac{\partial}{\partial r}\overline{pu} + \frac{\partial}{\partial x}\overline{pv}\right) + \upsilon\frac{\partial}{\partial r}\left\{\frac{1}{r}\frac{\partial}{\partial r}\left(r\frac{1}{2}\overline{uv}\right)\right\} - \varepsilon_{uv}, \tag{A7}$$

where ε_u, ε_v, ε_w, and ε_{uv} are the components of the homogeneous dissipation.

APPENDIX B: TRANSFORMED EQUATIONS

1. The momentum integral

Substitution of Eq. (3) into Eq. (A2) yields

$$U_s \delta^2 \int_0^\infty f\,\eta\,d\eta = U_\infty \theta^2. \tag{B1}$$

It follows immediately that if $\delta \equiv \delta_*$ and $U_s \equiv U_o$

$$\frac{U_s}{U_\infty} = \left[\frac{\theta}{\delta_*}\right]^2. \tag{B2}$$

2. The mean momentum and Reynolds stress equation

Substituting Eq. (3) into the momentum equation, Eq. (A1), and rearranging the terms yields

$$\left[\frac{\delta}{U_s}\frac{dU_s}{dx}\right] f - \left[\frac{d\delta}{dx}\right]\eta f' = \left[\frac{R_s}{U_\infty U_s}\right]\frac{(\eta g)'}{\eta} + \left[\frac{v}{U_\infty \delta}\right]\frac{(\eta f')'}{\eta}, \tag{B3}$$

where $'$ denotes derivation with respect to η. To this point the mean momentum equations have simply been transformed by the separation of variables in Eq. (3) so that all of the explicit x dependence is in the bracketed terms. Thus the results are completely general and no similarity assumptions have yet been made (although the form of the solutions has been restricted). Using Eq. (B1), Eq. (B3) can be rewritten as

$$-\left[\frac{d\delta}{dx}\right](\eta^2 f)' = \left[\frac{R_s}{U_\infty U_s}\right](\eta g)' + \left[\frac{v}{U_\infty \delta}\right](\eta f')'. \tag{B4}$$

Substituting Eq. (3) into the transport equations for Reynolds stresses yields:

$\overline{u^2}$-equation

$$\left[U_\infty \frac{dK_u}{dx}\right] k_u - \left[\frac{U_\infty K_u}{\delta}\frac{d\delta}{dx}\right]\eta k_u' = +\left[\frac{R_s U_s}{\delta}\right] f' g - \left[\frac{T_{u^2 v}}{\delta}\right]\frac{(\eta t_{u^2 v})'}{\eta} + [P_u]p_u - \left[\frac{dP_u^D}{dx}\right]p_u^D + \left[\frac{P_u^D}{\delta}\frac{d\delta}{dx}\right]\eta (p_u^D)' + \left[\frac{v K_u}{\delta^2}\right]\frac{(\eta k_u')'}{\eta} - [D_u]d_u, \tag{B5}$$

$\overline{v^2}$-equation

$$\left[U_\infty \frac{dK_v}{dx}\right] k_v - \left[\frac{U_\infty K_v}{\delta}\frac{d\delta}{dx}\right]\eta k_v' = -\left[\frac{T_{v^3}}{\delta}\right]\frac{(\eta t_{v^3})'}{\eta} + \left[\frac{T_{vw^2}}{\delta}\right]\frac{t_{vw^2}}{\eta} + [P_v]p_v - \left[\frac{P_v^D}{\delta}\right](p_v^D)' + \left[\frac{v K_v}{\delta^2}\right]\left(\frac{(\eta k_v')}{\eta}\right)' - [D_v]d_v, \tag{B6}$$

$\overline{w^2}$-equation

$$\left[U_\infty \frac{dK_w}{dx}\right] k_w - \left[\frac{U_\infty K_w}{\delta}\frac{d\delta}{dx}\right]\eta k_w' = -\left[\frac{T_{uw^2}}{\delta}\right]\frac{(\eta t_{uw^2})'}{\eta} - \left[\frac{T_{vw^2}}{\delta}\right]\frac{t_{vw^2}}{\eta} + [P_w]p_w + \left[\frac{v K_w}{\delta^2}\right]\left(\frac{(\eta k_w')}{\eta}\right)' - [D_w]d_w, \tag{B7}$$

$\overline{uv}$-equation

$$-\left[U_\infty \frac{dR_s}{dx}\right] g - \left[\frac{U_\infty R_s}{\delta}\frac{d\delta}{dx}\right]\eta g' = \left[\frac{K_v U_s}{\delta}\right] f' k_v - \left[\frac{T_{uv^2}}{\delta}\right]\frac{(\eta t_{uv^2})'}{\eta} + \left[\frac{T_{uw^2}}{\delta}\right]\frac{t_{uw^2}}{\eta} + [P_{uv}]p_{uv} - \left[\frac{P_u^D}{\delta}\right](p_u^D)' - \left[\frac{dP_v^D}{dx}\right](p_v^D) + \left[\frac{P_v^D}{\delta}\frac{d\delta}{dx}\right]\eta (p_v^D)' - \left[\frac{v R_s}{\delta^2}\right]\left(\frac{(\eta g)'}{\eta}\right)' - [D_{uv}]d_{uv}. \tag{B8}$$

As before, the equations have simply been transformed by the similarity transformations so that all the explicit x-dependence is in the bracketed terms.

APPENDIX C: A SOLUTION FOR A CONSTANT EDDY VISCOSITY MODEL

A solution of the momentum equation with the viscous term included [Eq. (A1)] can be obtained if an eddy viscosity assumption is made. Let

$$-\frac{1}{r}\frac{\partial}{\partial r}(r\overline{uv}) = v_T \frac{1}{r}\frac{\partial}{\partial r}\left(r\frac{\partial}{\partial r}(U - U_\infty)\right). \tag{C1}$$

Using Eq. (C1) and applying the similarity transformation, Eq (3), the governing equation in similarity form becomes

$$-\left[\frac{d\delta}{dx}\right](\eta^2 f)' = \left[\frac{\tilde{v}}{U_\infty \delta}\right]\frac{(\eta f')'}{\eta}, \tag{C2}$$

where $\tilde{v} = v + v_T$. Grouping the terms in square brackets, setting $k = (U_\infty \delta/\tilde{v})\partial\delta/\partial x$, results in the following differential equation:

$$(k\eta^2 f + \eta f')' = 0. \tag{C3}$$

The boundary conditions are $f(0) = 1$, $f(\infty) = 0$, and $f'(0) = f'(\infty) = 0$. Assuming that $f(\eta)$ goes to zero faster than a polynomial, the solution is given by

$$f(\eta) = e^{-k\eta^2/2}. \tag{C4}$$

Defining $\delta = \delta_*$, Eq. (B1), gives

$$\int_0^\infty f(\eta)\,\eta\, d\eta = 1, \tag{C5}$$

which is satisfied if $k = 1$. Then, the actual value of the eddy viscosity is given by

$$v_T = U_\infty \delta_* \frac{d\delta_*}{dx} - v. \tag{C6}$$

From the low local Reynolds number solution, Eq. (15), we have $\delta_* d\delta_*/dx = c^2/2R_\theta$, which finally results in $v_T = U_\infty c^2/2R_\theta - v$. The value of v_T can be estimated using the curve fit to the simulation of Gourlay *et al.*[13] In this simulation, $c = 1.90$, $U_\infty = 1$ m/s, $R_\theta = 1240$, and $v = 10^{-4}$ m^2/s, so $v_T = 1.35 \times 10^{-3}$ m^2/s. Thus $v_T/v = 13.5$, and this value is maintained throughout the low local Reynolds number similarity regime.

As noted by Johansson,[16,17] the simple exponential of the eddy viscosity solution is not a good fit to the high Reynolds number profile data, since it is too narrow near the centerline and falls off too slowly at large radius. Instead a curve was fitted to the data of the form

$$f(\eta) = (1 + a\eta^2 + b\eta^4)e^{(-c\eta^2 - d\eta^4)}, \tag{C7}$$

where $a = 0.049$, $b = 0.128$, $c = 0.345$, and $d = 0.134$. This curve is shown in Figs. 4, 13, and 15.

[1] T. Carmody, "Establishment of the wake behind a disk," J. Basic Eng. **86**, 869 (1964).
[2] N. C. H. Hwang and L. V. Baldwin, "Decay of turbulence in axisymmetric wakes," J. Basic Eng. **88**, 261 (1966).
[3] M. S. Uberoi and P. Freymuth, "Turbulent energy balance and spectra of the axisymmetric wake," Phys. Fluids **13**, 2205 (1970).
[4] P. M. Bevilaqua and P. S. Lykoudis, "Turbulence memory in self-preserving wakes," J. Fluid Mech. **89**, 589 (1978).
[5] A. A. Townsend, *The Structure of Turbulent Shear Flow* (Cambridge University Press, Cambridge, UK, 1956).
[6] A. A. Townsend, *The Structure of Turbulent Shear Flow*, 2nd ed. (Cambridge University Press, Cambridge, UK, 1976).
[7] S. C. Cannon, "Large-scale structures and the spatial evolution of wakes behind axisymmetric bluff bodies," Ph.D. thesis, Department of Aerospace and Mechanical Engineering, University of Arizona, 1991.
[8] Ö. İlday, H. Acar, M. Kubilay Elbay, and V. Atli, "Wakes of three axisymmetric bodies at zero angle of attack," AIAA J. **31**, 1152 (1992).
[9] C. Ostowari and R. H. Page, "Velocity defect of axisymmetric wakes," Exp. Fluids **7**, 284 (1989).
[10] J. L. F. Portiero and V. Perez-Villar, "Wake development in turbulent subsonic axisymmetric flows," Exp. Fluids **21**, 145 (1996).
[11] A. I. Sirviente and V. C. Patel, "Experiment in the turbulent near wake of an axisymmetric body," AIAA J. **37**, 1670 (1999).
[12] A. J. Basu, R. Narasimha, and U. N. Sinha, "Direct numerical simulation of the initial evolution of the axisymmetric wake," Curr. Sci. **63**, 734 (1992).
[13] M. J. Gourlay, S. C. Arendt, D. C. Fritts, and J. Werne, "Numerical modeling of initially turbulent wakes with net momentum," Phys. Fluids **13**, 3783 (2001).
[14] H. Schlichting, *Boundary-Layer Theory* (McGraw-Hill, New York, 1968).
[15] P. B. V. Johansson, W. K. George, and S. H. Woodward, "Proper orthogonal decomposition of an axisymmetric turbulent wake behind a disk," Phys. Fluids **14**, 2508 (2002).
[16] P. B. V. Johansson, "The axisymmetric turbulent wake," Ph.D. thesis, Chalmers University of Technology, Gothenburg, Sweden, 2002.
[17] P. B. V. Johansson and W. K. George, "The far downstream evolution of the high Reynolds number axisymmetric wake behind a disk. Part 1. Single point statistics," TRL Report No. 200, Chalmers University of Technology, 2002. Available at http://www.tfd.chalmers.se/trl.
[18] S. Cannon, F. Champagne, and A. Glezer, "Observations of large-scale structures in wakes behind axisymmetric bodies," Exp. Fluids **14**, 447 (1993).
[19] W. K. George, "The self-preservation of turbulent flows and its relation to initial conditions and coherent structures," in *Advances in Turbulence*, edited by W. K. George and R. E. A. Arndt (Hemisphere, New York, 1989), pp. 39–73.
[20] W. K. George, "Some new ideas for similarity of turbulent shear flows," in *Proc. ICHMT Symposium on Turbulence, Heat and Mass Transfer, Lisbon, Portugal (1994)*, edited by K. Hanjalic and J. C. F. Pereira (Begell, New York, 1995).
[21] I. Wygnanski, F. Champagne, and B. Marasli, "On the large-scale structures in two-dimensional, small-deficit, turbulent wakes," J. Fluid Mech. **168**, 31 (1986).
[22] H. Tennekes and J. L. Lumley, *A First Course in Turbulence* (MIT Press, Cambridge, MA, 1972).
[23] P. B. V. Johansson and W. K. George, "The far downstream evolution of the axisymmetric wake behind a disk. Part 2. Slice proper orthogonal decomposition," TRL Report No. 201, Chalmers University of Technology, 2002. Available at http://www.tfd.chalmers.se/trl.
[24] W. K. George, P. B. V. Johansson, and S. Gamard, "How has the study of coherent structures contributed to our understanding of turbulent free shear flows?" in 2002 ASME Fluid Engineering Division Summer Meeting, Montreal, Canada, 14–18 July 2002.
[25] W. K. George and L. Castillo, "Zero-pressure-gradient turbulent boundary layer," Appl. Mech. Rev. **50**, 689 (1997).
[26] R. D. Moser, M. M. Rogers, and D. W. Ewing, "Self-similarity of time-evolving plane wakes," J. Fluid Mech. **367**, 255 (1998).
[27] W. K. George and H. Wang, "The decay of confined turbulence," Bull. Am. Phys. Soc. **46**, 65 (2001).
[28] P. B. V. Johansson and W. K. George, "Application of equilibrium similarity analysis on the axisymmetric wake," in IUTAM Symposium on Bluff Body Wakes and Vortex-Induced Vibrations, Marseille, 13–16 June 2000.
[29] P. B. V. Johansson and W. K. George, "On the effect of finite Reynolds number and initial conditions on the axisymmetric wake," in *Turbulence and Shear Flow Phenomena II*, edited by E. Lindborg, A. Johansson, J. Eaton, J. Humphrey, N. Kasagi, M. Leschziner, and M. Sommerfeld (Stockholm, 27–29 June 2001) (KTH, Stockholm, Sweden), Vol. 1, pp. 323–328.